

OPEN ACCESS

Improved Performance of Silicon-Containing Anodes with Organic Solvent-Solubilized Lithium Nitrate

To cite this article: Leah Rynearson et al 2023 J. Electrochem. Soc. 170 060525

View the <u>article online</u> for updates and enhancements.

You may also like

- Improved Low Temperature Performance of Graphite/Li Cells Using Isoxazole as a Novel Cosolvent in Electrolytes Nuwanthi D. Rodrigo, Sha Tan, Zulipiya Shadike et al.
- Carbonate Free Electrolyte for Lithium Ion Batteries Containing -Butyrolactone and Methyl Butyrate
- Michael L. Lazar and Brett L. Lucht
- <u>Lithium Difluoro(oxalato)borate as Additive</u> to Improve the Thermal Stability of <u>Lithiated Graphite</u> Zonghai Chen, Yan Qin, Jun Liu et al.



244th ECS Meeting

Gothenburg, Sweden • Oct 8 – 12, 2023

Early registration pricing ends September 11

Register and join us in advancing science!



Learn More & Register Now!





Improved Performance of Silicon-Containing Anodes with Organic Solvent-Solubilized Lithium Nitrate

Leah Rynearson, D Chamithri Jayawardana, D Munaiah Yeddala, and Brett L. Lucht D

Department of Chemistry, University of Rhode Island, Kingston, Rhode Island 02881, United States of America

Three different organic solvents (dimethylacetamide (DMAc), dimethylformamide (DMF), and dimethyl sulfoxide (DMSO)) were used to improve the solubility of LiNO3 in a standard carbonate-based electrolyte with lithium difluoro(oxalato)borate (LiDFOB) as the salt. Together, the LiDFOB and organic-solvent solubilized LiNO3 preferentially reduce on the surface of silicon-containing anodes to create an SEI rich in oxalates, nitrate decomposition species, and B-F species. The improved stability of the SEI throughout the first 100 cycles results in silicon and silicon/graphite composite anodes with better capacity retention than observed with standard electrolytes or fluoroethylene carbonate (FEC) containing electrolytes. This study demonstrates the feasibility of the use of non-traditional electrolyte solvents in the improvement and optimization of lithium ion-battery electrolytes.

© 2023 The Author(s). Published on behalf of The Electrochemical Society by IOP Publishing Limited. This is an open access article distributed under the terms of the Creative Commons Attribution 4.0 License (CC BY, http://creativecommons.org/licenses/by/4.0/), which permits unrestricted reuse of the work in any medium, provided the original work is properly cited. [DOI: 10.1149/1945-7111/acdd26]

Manuscript submitted March 27, 2023; revised manuscript received May 31, 2023. Published June 19, 2023.

Supplementary material for this article is available online

Recently, there has been a large international push towards the electrification of vehicles with much interest and funding directed toward the development of long-lasting and robust batteries to further extend the driving range of electric vehicles (EV) towards that of the traditional combustion engine. A major limitation of designing lithium-ion batteries for these purposes is the size and weight requirements involved in building EVs as traditional lithiumion batteries rely on graphite anodes. While graphite is a stable anode with long cycle life, graphite has a relatively low specific capacity of 372 mAh g⁻¹, limiting the energy density of the battery. An alternative to this problem is utilizing alloying materials like silicon that have a very high theoretical capacity of 3579 mAh g⁻¹. However, upon lithiation, silicon undergoes a large volume expansion during the alloying process.² As the silicon particles expand, there is particle pulverization, electrical isolation, and continuous electrolyte decomposition leading to solid-electrolyte interphase (SEI) thickening over the course of the cycling period leading to poor capacity retention over time.3 One common approach to address this issue is to include small amounts of silicon nanoparticles in graphite electrodes which constrains the silicon volume changes but increases the overall capacity, and thus energy density, of the silicon-graphite composite electrode.

To further improve the cycling stability of silicon-containing anodes, many researchers have investigated the incorporation of additives into electrolyte formulations. Many of the electrolyte additives are reduced on the surface of the anode during the initial formation cycling to alter the composition and structure of the SEI resulting in improved performance. The electrolyte additives can limit some of the detrimental effects of volume expansion observed with silicon particles. For example, most researchers investigating silicon-containing anodes include fluoroethylene carbonate (FEC) as an additive, 3–10 wt% in LiPF₆/ethylene carbonate (EC)-based electrolytes. 4–6 This is because FEC has been shown to be preferentially reduced around 1.0-1.1 V vs Li/Li+ to form a stable, LiF-rich and polymer-rich SEI which is more resilient to the volumetric changes associated with silicon anodes during lithiation and delithiation.^{7,8} However, large quantities of FEC have been linked to gas evolution during cycling and can lead to the generation of HF upon cycling at elevated temperatures.^{9,10} In addition, FEC has been reported to continually degrade throughout the cycling process, and once consumed, the capacity of the cells decreases 11 Therefore, novel additives beyond FEC must be investigated to improve silicon-containing anode performance.

One potentially interesting electrolyte additive is LiNO₃. LiNO₃ has been utilized to stabilize lithium metal anodes in lithium sulfur batteries and is reduced on the anode surface to form a series of nitrogen containing species in the SEI which have been found to increase lithium-ion conduction and stabilize the SEI. 12–14 Since one of the major failure modes of silicon-containing anodes is the loss of electrical conductivity as a result of particle pulverization and thickening of the SEI, increased ion conductivity of the SEI throughout the course of cycling could lead to improved capacity retention as more anode particles will remain ionically conductive throughout cycling. Unfortunately, lithium nitrate is only sparingly soluble in standard carbonate electrolytes. Recent reports suggest that lithium nitrate improved the cycling stability of silicon-graphite composite electrodes. However, only concentrations of ~0.09 M LiNO₃ are soluble in 1.2 M LiPF₆ in EC:DEC (1:1). ¹⁵ An alternative approach to improving the cycling performance of silicon nanowire anodes utilizes LiNO₃ in a 1 M TFSI-based ether-based electrolyte. 16 Unfortunately, ethers are unstable at operating potentials of most common cathode materials and are thus problematic for most lithium-ion batteries. Previous investigations have reported on the improved performance with both lithium metal anodes and silicon/silicon-graphite composite anodes using an electrolyte of 1.0 M lithium difluoro(oxalato)borate (LiDFOB) in triethyl phosphate (TEP)/carbonate solvent blends with an overall LiNO₃ concentration of 0.2 M in the solution as a result of the high solubility of LiNO₃ in TEP. ^{17–19} The combination of LiDFOB and LiNO₃ were shown to generate stable SEI compositions that passivate the anode surface with oxalates, boron-fluorine containing species, and nitrate decomposition products. However, the solubility of LiNO₃ in TEP is limited, and TEP has been reported to inhibit stable SEI formation on graphite anodes leading to poor cycling performance, especially at high concentrations of TEP. 20,21 Similar problems are likely with silicon-graphite composite anodes. Therefore, other solvents should be investigated to improve the solubility of LiNO₃ and further optimize the promising LiDFOB+LiNO₃ electrolyte.

The solubility of lithium salts is typically higher in highly polar aprotic solvents, such as dimethylacetamide (DMAc), dimethylformamide (DMF), or dimethyl sulfoxide (DMSO). While these three solvents have traditionally not been utilized in high concentrations in lithium-ion battery electrolytes due to concerns related to the stability of the SEI, use of these solvents in lower concentrations to enable dissolution of LiNO₃ is an interesting possibility. Previous reports have utilized DMAc in both Li-air and Li-O₂ batteries. ^{22,23} While the use of DMAc has been generally limited in lithium-ion batteries, incorporation of DMAc as an additive into carbonate

electrolytes has been reported to lead to improved cycling performance as well as enhanced thermal stability, for LiPF₆ based electrolytes. He are also only been used sparingly in lithium-ion battery applications as a high temperature additive on LiFePO₄ cathodes with standard solvents. While there have been no literature reports of LiNO₃ solubilized in DMF, an SEI component formed as a result of LiNO₃ reduction, Li₃N, has been reported to be unreactive with DMF. Finally, DMSO has been used extensively with lithium metal anodes and can dissolve LiNO₃ to make a saturated solution with a high concentration of 4 M. Hold of the saturated DMSO solution of LiNO₃ to an FEC/carbonate based electrolyte can be used in Li/NCM811 cells which maintain 75% of the initial capacity after 200 cycles. Therefore, based on the promising cycling abilities and good LiNO₃ solubility, DMSO, DMF, and DMAc have been investigated in conjunction with the LiDFOB+LiNO₃ electrolyte as a substitute for TEP.

In this report, silicon anode half cells and silicon-graphite composite/NCM523 full cells were investigated with novel electrolyte formulations containing 1.0 M LiDFOB in EC:EMC with an overall LiNO $_3$ concentration \sim 0.24 M and either DMSO, DMF, or DMAc as a cosolvent. The novel electrolyte formulations were compared to a STD carbonate electrolyte and a STD carbonate electrolyte +3 wt% FEC. Ex-situ surface analysis was conducted with XPS after formation and after 100 cycles as well as FE-SEM imaging in order to investigate the changes in SEI morphology and chemical composition.

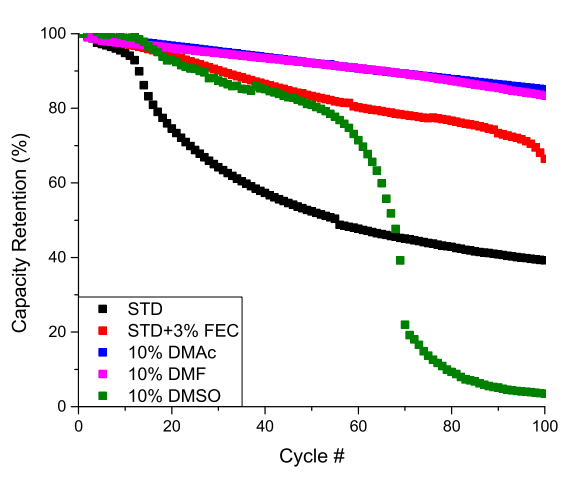
Experimental

Pure silicon anodes (Si) were made with silicon nanoparticles (≤50 nm) (Alfa-Aesar), Super C65 (Timcal), and poly(acrylic acid) (PAA) (MW = 450,000, Sigma-Aldrich) at a weight ratio of (50:25:25). Silicon-graphite composite electrodes (SiGr) were composed of silicon nanoparticles, artificial graphite (MTI Corporation), Super C65, and PAA in a 20:65:5:10 weight ratio. Anode material was mixed in a mortar and pestle for 1 h using water as a solvent before being transferred to a new vial and stirred using a magnetic stir bar for 3 h under vacuum. The homogenized slurry was spread onto copper foil using a doctor blade and air dried overnight. The anodes were punched into 14.0 mm diameter disks and dried in a vacuum oven overnight at 110 °C. The coating thickness for the pristine Si anodes was \sim 19 μ m and for the pristine SiGr anodes, the thickness was $\sim 33 \,\mu\text{m}$. Neither handmade anode was calendared. The cathodes were $LiNi_{0.5}Co_{0.2}Mn_{0.3}O_2$ (NCM523) single side coated electrodes (MTI Corporation) with 94.2% active material and 5.8% conductive carbon and polyvinylidene difluoride (PVdF). Cathodes were punched into 12.7 mm disks and dried at 110 °C overnight in a vacuum oven. The N/P ratio between the SiGr anode and NCM523 cathode was calculated to be 1.14.

Electrolytes investigated include: 1.2 M LiPF₆ in ethylene carbonate (EC):ethyl methyl carbonate (EMC) (3:7, v/v) (STD electrolyte), 1.2 M LiPF₆ in EC:EMC with 3 wt% fluoroethylene carbonate (FEC) (STD + 3% FEC electrolyte), 1.0 M LiDFOB in dimethylacetamide saturated with LiNO3:EC:EMC (estimated 0.24 M LiNO₃ in 1:1:8) (10% DMAc electrolyte), 1.0 M LiDFOB in dimethylformamide saturated with LiNO3:EC:EMC (estimated 0.24 M LiNO₃ in 1:1:8) (10% DMF electrolyte), 1.0 M LiDFOB in dimethyl sulfoxide saturated with LiNO3:EC:EMC (estimated 0.19 M LiNO₃ in 1:1:8) (10% DMSO electrolyte). The 1.2 M LiPF₆ in EC:EMC (3:7) and LiDFOB were obtained from BASF. Battery grade FEC, EC, and EMC were supplied by Gotion, Inc. The LiNO₃ and dimethylacetamide (99%, dried over molecular sieves) were purchased from Sigma-Aldrich. The dimethyl sulfoxide (99.8+ %, anhydrous, dried over molecular sieves) was purchased from Fisher Scientific and the dimethylformamide (99.8%, anhydrous, dried over molecular sieves) from Acros.

Coin cells (2032) were prepared inside an Ar-glovebox. Si/Li half cells consist of a Si working electrode, lithium foil counter electrode, 100 μ l of electrolyte, one Celgard 2325 separator, and one Whatman GF/D glass microfiber separator. SiGr/NCM523 full cells consist of a SiGr anode, NCM523 cathode, 100 μ l of electrolyte, two Celgard 2325 separators, and one Whatman GF/D glass microfiber separator. Half cells were cycled between 0.005 V and 1.5 V and full cells were cycled between 3.0 V and 4.2 V. All cells had the same cycling procedure: C/20 for the first cycle, C/10 for the next two cycles, and C/5 for an additional 97 cycles with the first five cycles considered formation cycling. Cells were cycled at 25 °C using an Arbin BT2000 battery cycler. The rate for half-cells was calculated based on the theoretical capacity of Si at 3579 mAh g $^{-1}$. Full cell capacity and rate were calculated based on the mass of cathode active material. All cells were built in triplicate with representative data provided.

After cycling was completed, delithiated electrodes were removed from the disassembled cells and rinsed with three portions of 675 μ l of dimethyl carbonate (DMC) in order to remove any excess electrolyte. Electrodes were then dried in an argon-filled glove box for further ex situ surface analysis. Surface analysis was performed using ex situ X-ray photoelectron spectroscopy (XPS) (K-alpha, Thermo) with an Al K\alpha X-ray source at a pass energy of 50 eV and a measured spot size of 400 μ m. Electrodes were transferred to the XPS chamber without exposure to air using a vacuum-sealed transfer module (Thermo). The binding energy was corrected based on the C1s peak for hydrocarbon at 284.8 eV. The change in electrode surface morphology throughout cycling was examined using ex situ field-emission scanning electron microscopy (Zeiss Sigma VP) equipped with energy dispersive X-ray spectroscopy (Oxford Instruments) (FE-SEM-EDS) at 20.00 kV.



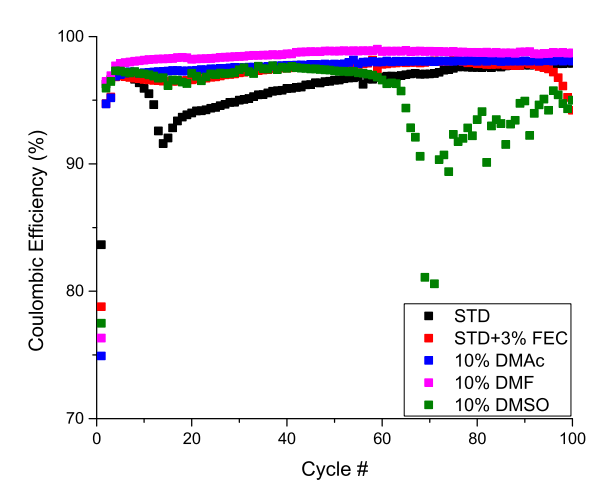


Figure 1. (left) Capacity retention vs cycle # and (right) coulombic efficiency vs cycle # of Si/Li half cells cycled with electrolytes of interest.

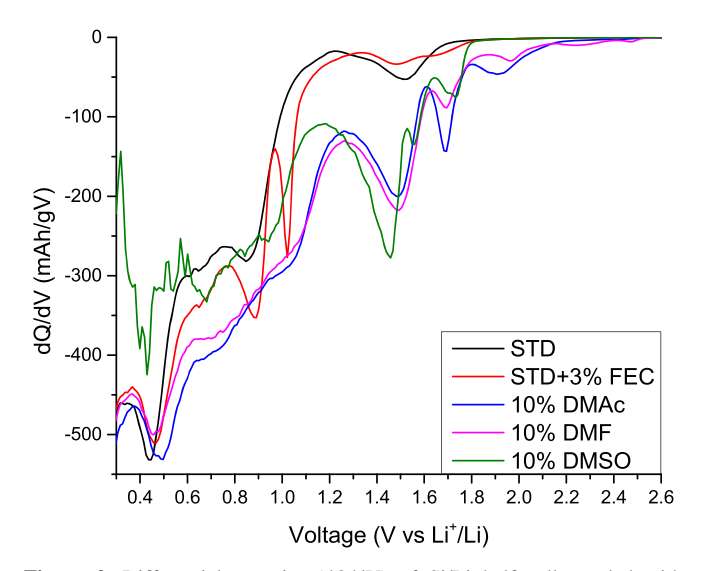


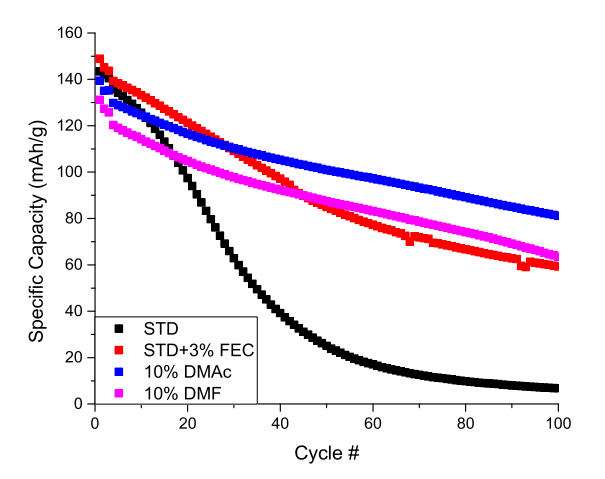
Figure 2. Differential capacity (dQ/dV) of Si/Li half cells cycled with electrolytes of interest during first lithiation.

Results and Discussion

Electrochemical cycling.—The coulombic efficiency and capacity retention of Si/Li half cells cycled with the five electrolytes of interest are provided in Fig. 1. Due to the low quantity of silicon active material on each electrode and the variations in current collector mass, the capacity of the silicon electrodes has been normalized to the first cycle charge capacity for better depiction of cycling stability. ³¹ All Si anodes exhibit an initial specific capacity >3200 mAh g⁻¹. While the cells cycled with the STD electrolyte had the highest initial coulombic efficiency, there is a sudden drop in capacity around the 15th cycle leading to a consistent decrease throughout the cycling period and ending in a capacity retention of 39.2%. The cells cycled with the STD+3% FEC electrolyte have good initial cycling stability, but the capacity steadily decreases during cycling, eventually retaining only 66.4% of the initial capacity after 100 cycles. Of the three LiNO₃-containing electrolytes, the cells cycled with the 10% DMSO electrolyte have the highest first cycle coulombic efficiency but exhibit unstable cycling including a sharp drop-off in capacity beginning around the 60th cycle, ending in near complete cell failure and rapidly fluctuating coulombic efficiencies. The poor electrochemical performance is likely attributed to the lower calculated concentration of LiNO₃, the high affinity of DMSO for water, and the solubility of SEI components in DMSO. The cells cycled with the 10% DMF and 10% DMAc electrolytes have relatively similar cycling stability for

the majority of the 100 cycles with the 10% DMF electrolyte having a slightly higher coulombic efficiency but ending with a slightly lower capacity retention (83.4%) than the 10% DMAc electrolyte (85.1%).

The differential capacity (dQ/dV) plots from the first cycle lithiation in the region of 0.3-2.6 V of the Si/Li half cells are provided in Fig. 2. As previously reported, all cells containing the pure silicon anodes exhibit a peak around 0.43 V vs Li/Li⁺ due to the partial reduction of the native SiO_2 layer formed as a result of manual electrode preparation. While the cell cycled with the 10% DMSO electrolyte might have a peak in that region, the noisy peaks are consistent with an instability of the electrode with the electrolyte causing continuous electrolyte decomposition, which is reflected in unstable cycling and cell failure as depicted in Fig. 1. The partial reduction of the PAA binder can be seen at \sim 1.5 V vs Li/Li $^+$ for the STD and STD+3% FEC electrolytes, $\sim\!\!1.48\,V$ vs Li/Li⁺ for the cells cycled with the 10% DMAc and 10% DMF electrolytes, and ~1.44 V vs Li/Li⁺ for the cell cycled with the 10% DMSO electrolyte. The shifting in the reduction peak can be attributed to differences in solvent-salt interactions. In the cells cycled with the STD and STD+3% FEC electrolytes, the peak characteristic of EC reduction is distinct at ~0.89 V vs Li/Li⁺ whereas the cells cycled with LiDFOB/LiNO3-containing electrolytes have much less EC reduction which has been shifted closer to 1.03 V vs Li/Li⁺.33 Due to the preferential reduction of LiDFOB and LiNO₃, the majority of the silicon anode surface is passivated prior to the EC reduction potential leading to less EC reduction on the silicon anode surface. The cell cycled with STD+3% FEC has an additional peak around $1.01\,\mathrm{V}$ vs $\mathrm{Li/Li^+}$ as a result of FEC reduction. ¹⁵ The peak at $\sim 1.69\,\mathrm{V}$ vs $\mathrm{Li/Li^+}$ in the 10% DMAc, 10% DMF, and 10% DMSO electrolytes is consistent with LiDFOB reduction. 34 Of the three solvents, DMAc has the largest intensity reduction peak indicating that LiDFOB is the primary contributor to the SEI for the 10% DMAc electrolyte. The 10% DMSO has a small peak which is consistent with poor SEI generation and cycling stability. There are multiple LiNO₃ reduction peaks in the cells cycled with 10% DMF and 10% DMAc electrolyte in the region between 1.90–2.24 V vs Li/Li⁺. 15,35 While the 10% DMF electrolyte has a smaller LiDFOB reduction peak than observed with the 10% DMAc electrolyte, the presence of multiple LiNO₃ reduction peaks demonstrate the importance of both components being present in the electrolyte solution. The cell cycled with 10% DMSO does not appear to exhibit any LiNO3 reduction peaks, possibly due to the increased solubility of LiNO₃ decomposition products in DMSO. The lack of one of the preferentially reducing SEI components contributing to initial SEI growth likely contributes to rapid cell failure as observed for the cells cycled with 10% DMSO electrolyte. Due to the poor cycling performance, further investigation of the 10% DMSO electrolyte was not conducted.



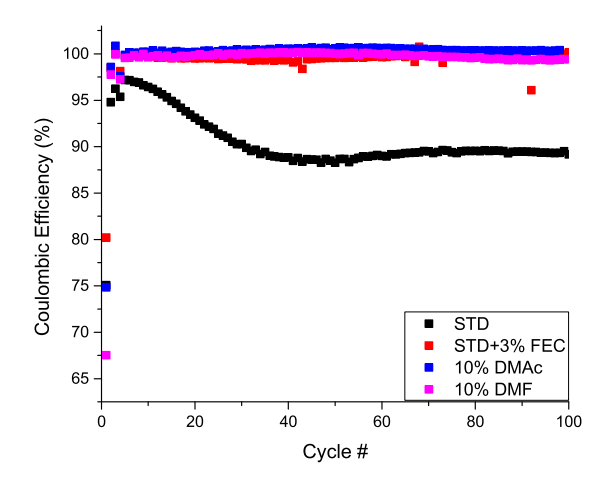


Figure 3. (left) Specific capacity vs cycle # and (right) coulombic efficiency vs cycle # of SiGr/NCM523 full cells cycled with electrolytes of interest.

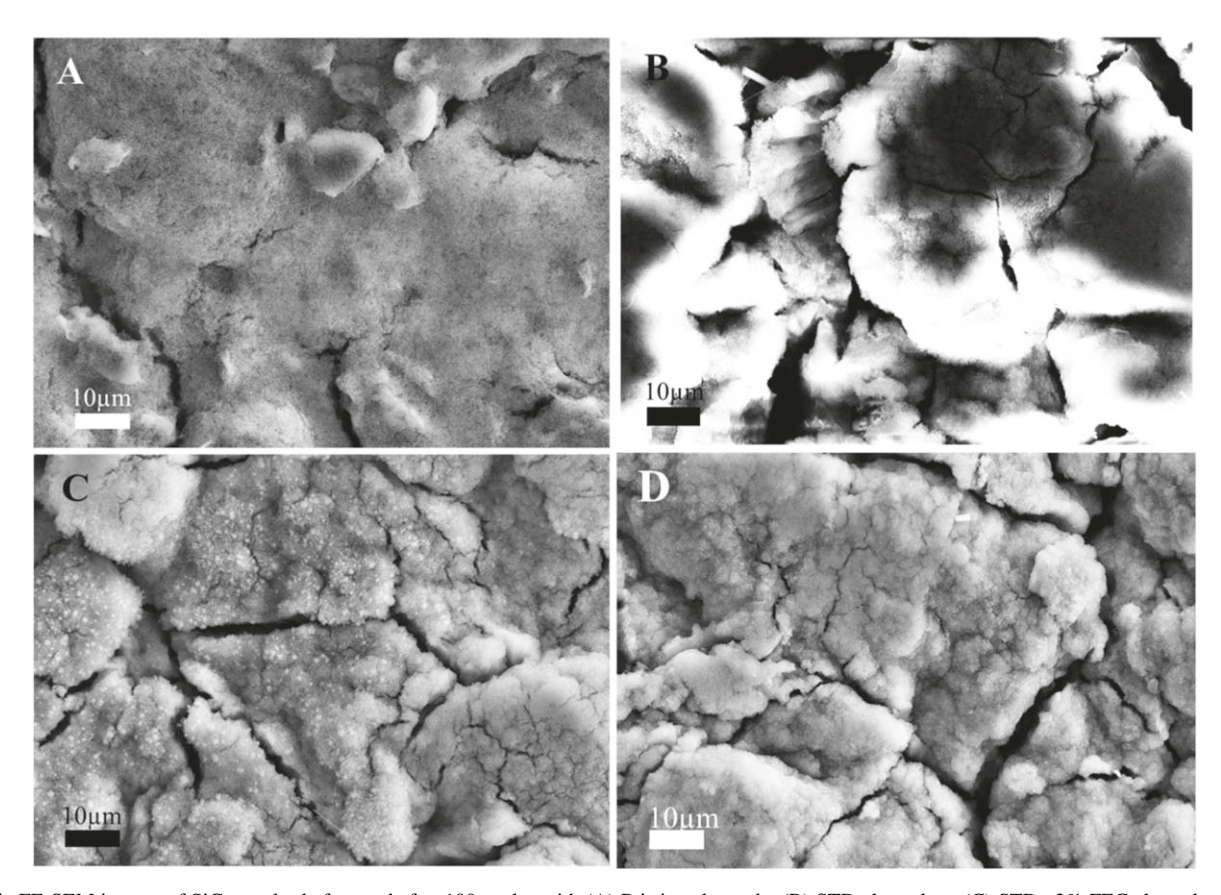


Figure 4. FE-SEM images of SiGr anodes before and after 100 cycles with (A) Pristine electrode, (B) STD electrolyte, (C) STD+3% FEC electrolyte, and (D) 10% DMAc electrolyte at 2500X.

The specific capacity vs cycle number and coulombic efficiency vs cycle number of the SiGr/NCM523 full cells are plotted below in Fig. 3. The voltage vs charge/discharge specific capacity of the SiGr/ NCM523 cells cycled with the four electrolytes for the first and 100th cycle are plotted in Fig. S1. The cells cycled with the STD electrolyte exhibit poor cycling performance and lose nearly all capacity by the 60th cycle. This is further reflected in the low coulombic efficiency (<95%) throughout the entire cycling period. Cycling with the STD+3% FEC gives better initial capacities; however, there is a continuous decrease in capacity throughout the cycling period with a steeper decrease between the 25th and 45th cycles. This leads to an ending capacity of 58 mAh g⁻¹ after 100 cycles. While the Si/Li half cells cycled with the 10% DMF and 10% DMAc electrolytes exhibited very similar cycling behavior, the SiGr/NCM523 full cells have larger differences. The cell cycled with 10% DMF has a lower initial capacity as well as a lower first cycle coulombic efficiency and exhibited a slightly steeper capacity fade over the cycling period than that seen with the 10% DMAc electrolyte leading to a final capacity of 63 mAh g⁻¹, which is only slightly better than the capacity observed by cycling with the STD +3% FEC electrolyte. The cells cycled with the 10% DMAc electrolyte have a slightly lower initial specific capacity than the STD+3% FEC electrolyte but have better capacity retention upon cycling retaining 81 mAh $\rm g^{-1}$ (59%) after 100 cycles. The differences in cycling between the 10% DMF and 10% DMAc electrolytes is likely due to varying electrolyte dynamics as a result of the solvent change. A rate capability test was performed on the cells cycled with the STD, STD+3% FEC, and 10% DMAc electrolytes and is displayed in Fig. S2. Cycling with the STD electrolyte gave the largest amount of capacity loss between the initial and final capacity, especially at higher rates. The STD+3% FEC had the highest capacity across the entire cycling rate period; however, the cell starts to exhibit higher capacity fade in the return to the C/5 cycling than

the cell cycled with 10% DMAc. While the cell cycled with 10% DMAc does have lower capacities than the cell cycled with the STD +3% FEC electrolyte, there is greater capacity retention from beginning to end of cycling, even at high rates. Based on the better cycling performance, the 10% DMAc electrolyte was selected for further analysis in comparison to the two STD-based electrolytes.

FE-SEM-EDS Images.—In order to examine the differences in the SiGr anodes before and after 100 cycles in the SiGr/NCM523 full cells, ex situ FE-SEM-EDS was performed on the anodes extracted from the cells cycled with the electrolytes of interest (Fig. 4) with the EDS elemental maps presented in Figs. S3–S6. The pristine electrode has a fairly uneven surface due to relative size scale differences between the nanoparticle-sized silicon and micrometer-sized graphite where the larger graphite particles are embedded in a silicon particle and PAA matrix. Observations of the SEI morphology in relation to the distinct features of the silicon nanoparticles in the pristine electrode thus allow for an idea of the physical changes caused by electrolyte decomposition. The anode cycled with the STD electrolyte is covered with a thick SEI as evidenced by the disappearance of silicon nanoparticles. There are also severe charging effects due to delamination of electrode material from the copper current collector. This further reflects the cell failure observed in the cycling data. Cycling the SiGr electrode with the STD+3% FEC electrolyte generates uneven SEI coverage as seen by the granular structures on some portions of the electrode and thicker carbonate coverage in other sections. EDS analysis of this electrode is consistent with granular structures composed of LiF and bulk coverage with lithium alkyl carbonates (Fig. S5). FEC has been reported to generate large quantities of LiF on silicon electrodes which are then covered with carbonate decomposition products upon additional cycling.⁸ The uneven distribution suggests that there is not sufficient FEC in the electrolyte to fully passivate

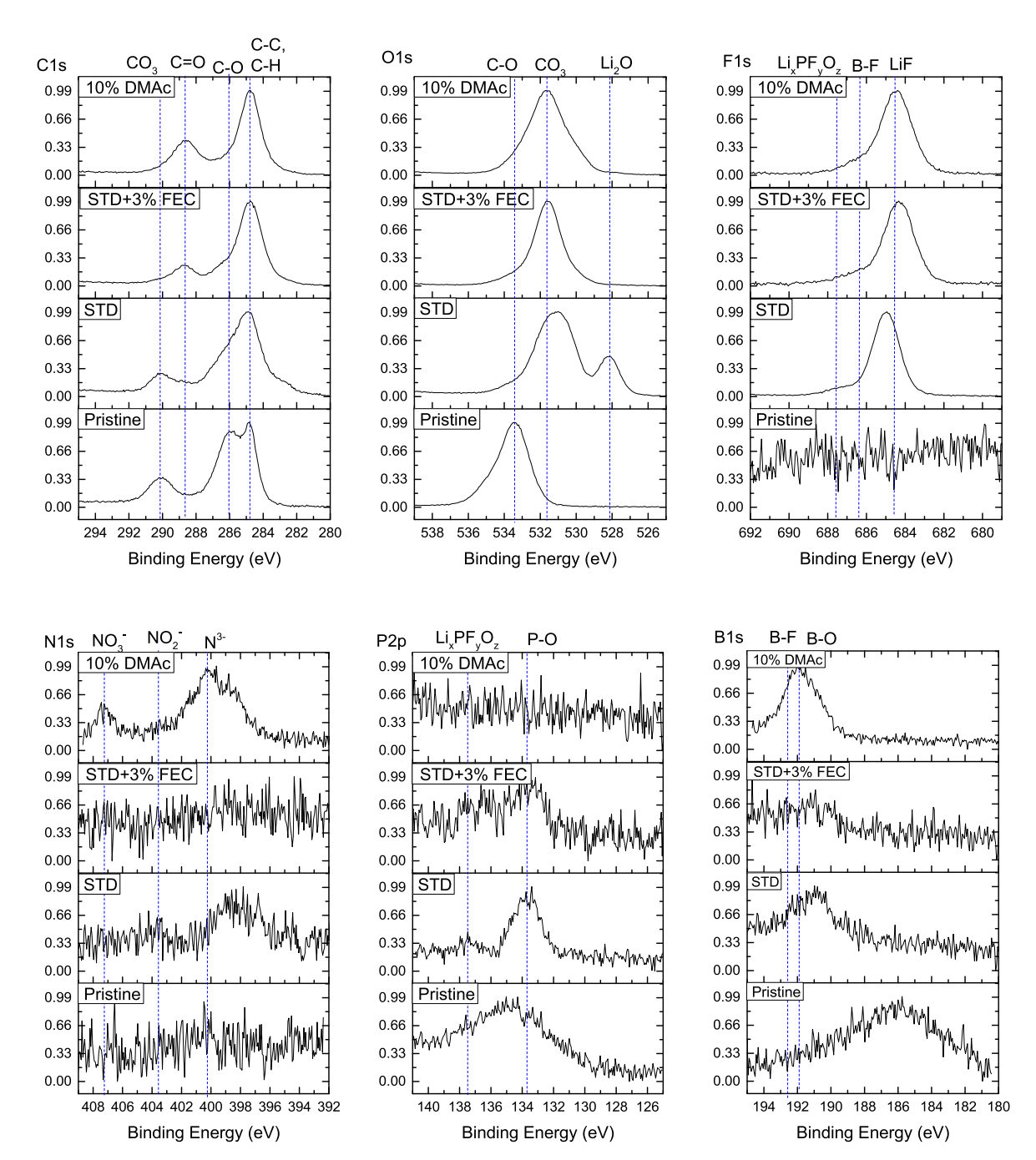


Figure 5. C1s, O1s, F1s, N1s, P2p, and B1s XPS spectra of SiGr anodes extracted from SiGr/NCM523 full cells after formation cycling.

the surface via reduction of the FEC which is consistent with the slow and steady capacity loss. The anode cycled with the 10% DMAc electrolyte has thick but even SEI growth leading to relatively consistent coverage of the oxalate, nitrate, and borate products as discussed below with the analysis of the XPS spectra and visualized in Fig. S6.

XPS analysis of anodes after formation cycling.—The C1s, O1s, F1s, N1s, P2p, and B1s XPS spectra of the SiGr anode from the SiGr/NCM523 full cells after formation cycling with the electrolytes of interest are provided in Fig. 5. Peaks are observed at 284.8 eV in the C1s spectrum of the pristine SiGr anode due to the presence of adventitious carbon and graphite while additional peaks are observed at 286.1 eV (C–O) and 290 eV (CO₂) due to the presence of the PAA binder in the anode. Cycling with the STD electrolyte results in the appearance of new peaks in the XPS spectra at 531.8 eV in the O1s

spectrum and 290.1 eV in the C1s spectrum characteristic of lithium alkyl carbonates and Li₂CO₃. Additional peaks are observed at 685 eV in the F1s spectrum, 528 eV in the O1s spectrum, and at 687.5 eV in the F1s spectrum and 133.7 eV/137.5 eV in the P2p spectrum, consistent with the presence of LiF, Li₂O, and Li_xPF_vO_z, respectively. The presence of these species in the SEI is consistent with previous reports.^{3,19,36} Cycling with the STD+3% FEC electrolyte primarily generates lithium carboxylates or oxalates based on the higher concentrations of C=O and C-O observed and the very weak peak for CO₃ species in the C1s spectrum. Interestingly, no Li₂O is observed. There also appears to be some LiF present with very little Li_xPF_vO_z formed as evidenced by the small shoulder at 687 eV in the F1s spectrum and very weak peak at 133.5 eV in the P2p spectrum. The 10% DMAc electrolyte generates an SEI consisting of oxalates (with the strong peaks of C=O and C-O) as well as some B-F containing compounds as evidenced by

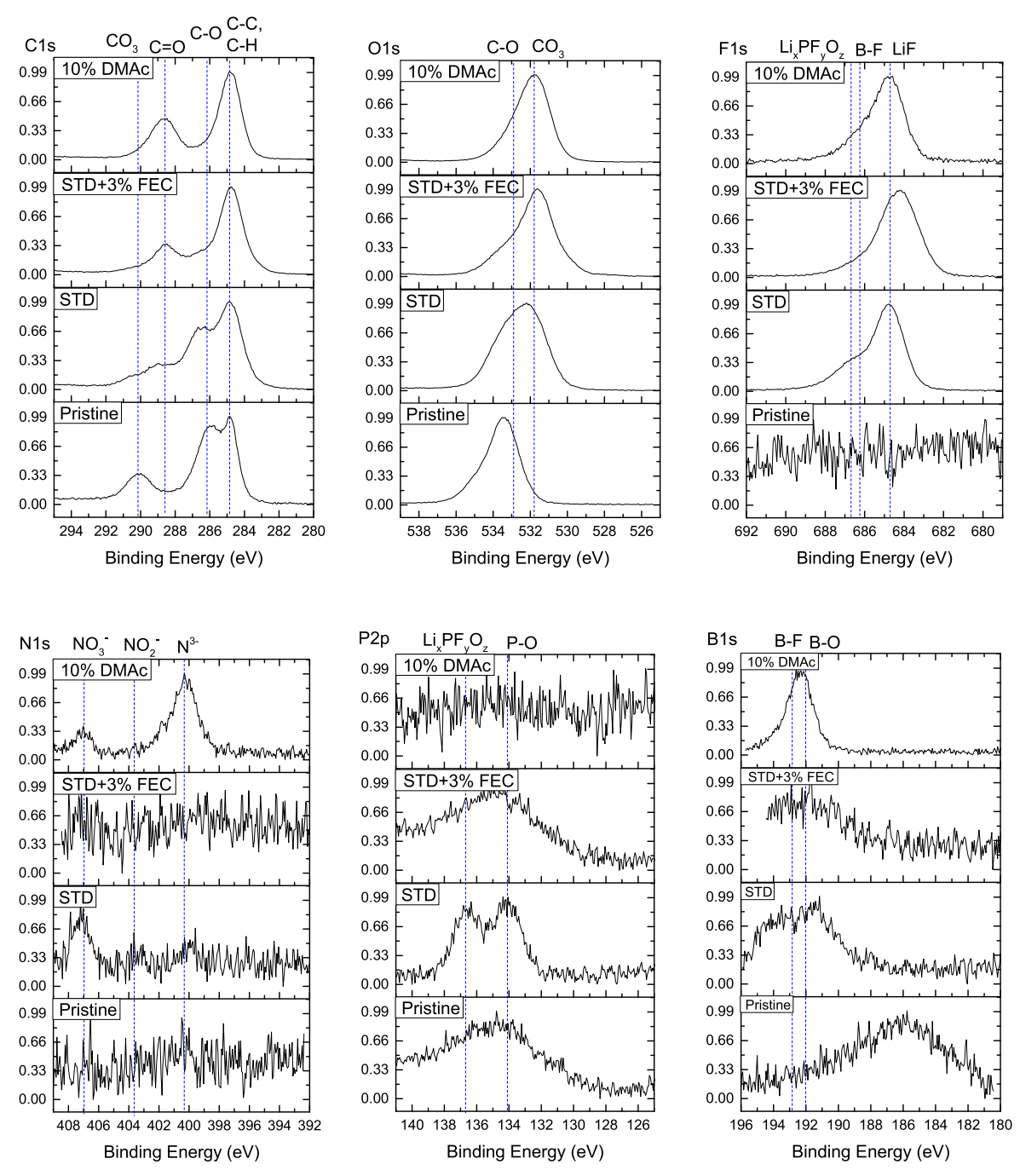


Figure 6. C1s, O1s, F1s, N1s, P2p, and B1s XPS spectra from SiGr anodes extracted from SiGr/NCM523 full cells after 100 cycles.

		C	O	F	N	P	В
	Pristine	42.7	30.1				
After Formation	STD	38.3	41.7	17.9		1.1	
	STD+3% FEC	52.9	37.7	8.2			
	10% DMAc	40.9	39.5	9.9	2.7		6.9
After 100 Cycles	STD	45.5	30.7	22.0		1.8	
	STD+3% FEC	51.4	31.2	16.7		0.7	
	10% DMAc	44.8	39.4	5.4	2.1		8.3

the peaks at 686.5 eV in the F1s spectrum and 192.8 eV in the B1s spectrum. 36,37 Furthermore, the LiNO₃ has decomposed to form primarily N^{3-} and NO_{3}^{-} products with very little NO_{2}^{-} present.

XPS analysis of the anodes after 100 cycles.—The C1s, O1s, F1s, N1s, P2p, and B1s XPS spectra of the SiGr anodes extracted from the SiGr/NCM523 full cells after 100 cycles with the electrolytes of interest are displayed in Fig. 6. Cycling with the STD electrolyte for a longer period generates even more lithium carbonate and lithium alkyl carbonates as seen by the increased intensity of the C=O (288.9 eV) and C-O (286 eV) signals. The Li₂O observed at the end of formation cycling has now been covered as evidenced by an increased concentration of LiF (684.8 eV) and Li_xPF_vO_z (686.7 eV in the F1s and 136.9 eV in the P2p spectra), consistent with continuous SEI growth throughout the cycling period. This is due to repeated electrolyte degradation which results in poor cycling behavior as presented above. The cells cycled with the STD+3% FEC electrolyte have a relatively similar SEI to that observed after formation cycling. There is a slightly higher concentration of C-O and C=O species as seen by an increased shoulder in the O1s spectrum at 533 eV and a higher concentration of C-O at 286 eV and C=O at 288.6 eV than seen previously. Furthermore, there is continued growth of the peaks associated with LiF and Li_xPF_yO_z in the F1s spectrum, although there is no longer any clear signal in the P2p spectrum. The continued strong presence of LiF even after extended cycling contrasts the layering that has been observed in previous investigations of higher weight percentages of FEC. 18,19,38 Cycling with the 10% DMAc electrolyte for 100 cycles results in an SEI very similar to that observed after formation cycling. There is slightly more oxalate formation as evidenced by the increased C=O peak at 288.8 eV in the C1s spectrum and more B-F species generated as indicated by the higher intensity of the signal at 686.2 eV in the F1s and 192.8 eV in the B1s spectrum. This is consistent with continued LiDFOB decomposition over the course of cycling as previously reported.^{36,39} In addition, there is an increase in LiNO₃ decomposition species, especially N₃⁻ at 400.2 eV. The lack of significant changes in proportions of the SEI components between formation cycling and after 100 cycles in the DMAc electrolyte indicates that the initial SEI formed is relatively stable and consistent throughout and that there is not significant electrolyte degradation occurring during continued cycling.

XPS elemental percentages.—To develop a better understanding of the SEI evolution across the cycling period, the XPS spectra of the SiGr anodes discussed earlier were used to calculate a relative elemental percentage for each species with the results displayed in Table I. The pristine electrode contains high concentrations of C and O as a result of the graphite and binder used in the electrode. Although not displayed in the table due to brevity, the pristine electrode had a relative elemental percentage of Si of 27.2%. The cell cycled with the STD electrolyte exhibits a large increase in C and F species, a small increase in P, and a decrease in O. This is consistent with the SEI evolution discussed above with greater lithium carbonate and LixPFvOz species generated. Cycling with the STD+3% FEC electrolyte maintains relatively consistent C concentrations during cycling with a decrease in O species and an increase in F species. The increase in F species is different than typically observed with high concentrations of FEC where an inorganic LiF-dominated layer is formed during formation cycling that is then covered by more organic carbonate-based species over the course of cycling.³ Since there is less FEC in solution, the solvent dynamics may have changed leading to less FEC available for reduction. The cell cycled with 10% DMAc electrolyte remains relatively similar across the cycling period with a small increase in C and B species, a decrease in F species, and the O and N species staying generally consistent. This further corroborates the idea that there is continued LiDFOB decomposition during the first 100 cycles; however, the SEI remains relatively unchanged since the formation cycling indicating that the initial electrolyte decomposition is enough to nearly passivate the surface.

Conclusions

The cycling stability of both silicon and silicon-graphite composite anodes can be improved over what is observed for STD carbonate electrolytes through the inclusion of sacrificial additives. While FEC is the most frequently reported electrolyte additive which results in the generation of a LiF and polymer-rich SEI, the STD +3% FEC electrolyte was unable to outperform either the 10% DMAc or the 10% DMF electrolytes, likely due to the presence of both LiDFOB and LiNO3 in a solvent that is able to dissolve LiNO3 up to $\sim 0.24 \,\mathrm{M}$. Further ex situ analysis of the 10% DMAc electrolyte reveals a stable SEI consisting of oxalates, B-F species. and N₃ species that remains relatively unchanged throughout the 100 cycles. These results demonstrate the use of non-traditional lithium-ion battery solvents to further improve the properties of an electrolyte for silicon-containing anodes in order to generate improved cycling capabilities.

Acknowledgments

This material is based upon work supported by the U.S. Department of Energy, Office of Science, EPSCoR National Laboratory Partnership Program, under Award Number DE-SC0021392. The SEM data was acquired at the RI Consortium for Nanoscience and Nanotechnology, a URI College of Engineering core facility partially funded by the National Science Foundation EPSCoR, Cooperative Agreement #OIA-1655221.

ORCID

Leah Rynearson https://orcid.org/0000-0003-3472-7630 Chamithri Jayawardana https://orcid.org/0000-0002-3144-6377 Brett L. Lucht https://orcid.org/0000-0002-4660-0840

References

- 1. T. D. Hatchard and J. R. Dahn, "In situ XRD and electrochemical study of the reaction of lithium with amorphous silicon." J. Electrochem. Soc., 151, A838
- 2. M. N. Obrovac and L. Christensen, "Structural changes in silicon anodes during
- lithium insertion/extraction." *Electrochem. Solid-State Lett.*, **7**, A93 (2004).

 M. Nie, D. P. Abraham, Y. Chen, A. Bose, and B. L. Lucht, "Silicon solid electrolyte interphase (SEI) of lithium ion battery characterized by microscopy and spectroscopy." J. Phys. Chem. C, 117, 13403 (2013).
- 4. I. A. Shkrob, J. F. Wishart, and D. P. Abraham, "What makes fluoroethylene carbonate different?" J. Phys. Chem. C, 119, 14954 (2015).
- 5. T. R. Martin, L. Rynearson, M. Kuller, J. Quinn, C. Wang, B. L. Lucht, and N. Neale, "Conjugated imine polymer synthesized via step-growth metathesis for highly stable silicon nanoparticle anodes in lithium-ion batteries." Adv. Energy Mater., 13, 2203921 (2023).
- 6. D. Mazouzi et al., "Insights into the silicon-based electrode's irreversibility along cycle life through simple gravimetric method." J. Power Sources, 220, 180 (2012).
- 7. A. L. Michan, B. S. Parimalam, M. Leskes, R. N. Kerber, T. Yoon, C. P. Grey, and B. L. Lucht, "Fluoroethylene carbonate and vinylene carbonate reduction: understanding lithium-ion battery electrolyte additives and solid electrolyte interphase formation." Chem. Mater., 28, 8149 (2016).
- 8. C. Xu, F. Lindgren, B. Philippe, M. Gorgoi, F. Björefors, K. Edström, and T. Gustafsson, "Improved performance of the silicon anode for li-ion batteries: understanding the surface modification mechanism of fluoroethylene carbonate as an effective electrolyte additive." Chem. Mater., 27, 2591 (2015).
- 9. A. Schiele, B. Breitung, T. Hatsukade, B. B. Berkes, P. Hartmann, J. Janek, and T. Brezesinski, "The critical role of fluoroethylene carbonate in the gassing of silicon anodes for lithium-ion batteries." ACS Energy Lett., 2, 2228 (2017).
- 10. K. Kim, I. Park, S.-Y. Ha, Y. Kim, M.-H. Woo, M.-H. Jeong, W. C. Shin, M. Ue, S. Y. Hong, and N.-S. Choi, "Understanding the thermal instability of fluoroethylene carbonate in LiPF₆-based electrolytes for lithium ion batteries." Electrochim. Acta, 225, 358 (2017).
- 11. R. Jung, M. Metzger, D. Haering, S. Solchenbach, C. Marino, N. Tsiouvaras, C. Stinner, and H. A. Gasteiger, "Consumption of fluoroethylene carbonate (FEC) on Si-C composite electrodes for li-ion batteries." J. Electrochem. Soc., 163, A1705
- 12. Y. Liang, W. Wu, D. Li, H. Wu, C. Gao, Z. Chen, L. Ci, and J. Zhang, "Highly stable lithium metal batteries by regulating the lithium nitrate chemistry with a modified eutectic electrolyte." Adv. Energy Mater., 12, 2202493 (2022).
- 13. R. May, K. J. Fritzsching, D. Livitz, S. R. Denny, and L. E. Marbella, "Rapid interfacial exchange of li ions dictates high coulombic efficiency in li metal anodes." ACS Energy Lett., 6, 1162 (2021).
- 14. A. Jozwiuk, B. B. Berkes, T. Weiβ, H. Sommer, J. Janek, and T. Brezesinski, "The critical role of lithium nitrate in the gas evolution of lithium-sulfur batteries." Energy Environ. Sci., 9, 2603 (2016).

- C. C. Nguyen and B. L. Lucht, "Development of electrolytes for Si-graphite composite electrodes." J. Electrochem. Soc., 165, A2154 (2018).
- V. Etacheri, O. Haik, Y. Goffer, G. A. Roberts, I. C. Stefan, R. Fasching, and D. Aurbach, "Effect of fluoroethylene carbonate (FEC) on the performance and surface chemistry of si-nanowire li-ion battery anodes." *Langmuir*, 28, 965 (2012).
- Z. L. Brown, S. Heiskanen, and B. L. Lucht, "Using triethyl phosphate to increase the solubility of LiNO₃ in carbonate electrolytes for improving the performance of the lithium metal anode." *J. Electrochem. Soc.*, 166, A2523 (2019).
- L. Rynearson, N. D. Rodrigo, C. Jayawardana, and B. L. Lucht, "Electrolytes containing triethyl phosphate solubilized lithium nitrate for improved silicon anode performance." J. Electrochem. Soc., 169, 040537 (2022).
- L. Rynearson, C. Jayawardana, N. D. Rodrigo, and B. L. Lucht, "Improved SiGr/ NCM523 Cycling via Triethyl Phosphate-Solubilized Lithium Nitrate Electrolyte." J. Phys. Chem. C, 127, 1755 (2023).
- K. Xu, M. S. Ding, S. Zhang, J. L. Allen, and T. R. Jow, "An attempt to formulate nonflammable lithium ion electrolytes with alkyl phosphates and phosphazenes." *J. Electrochem. Soc.*, 149, A622 (2002).
- K. Xu, S. Zhang, J. L. Allen, and T. R. Jow, "Nonflammable electrolytes for Li-Ion batteries based on a fluorinated phosphate." *J. Electrochem. Soc.*, 149, A1079 (2002).
- F. Wang, H. Chen, Q. Wu, R. Mei, Y. Huang, X. Li, and Z. Luo, "Study on the mixed electrolyte of N,N-dimethylacetamide/sulfolane and its application in aprotic lithium-air batteries." ACS Omega, 2, 236 (2017).
- W. Walker, V. Giordani, J. Uddin, V. S. Bryantsev, G. V. Chase, and D. Addison, "A rechargeable Li-O₂ battery using a lithium nitrate/N,N-dimethylacetamide electrolyte." *J. Am. Chem. Soc.*, 135, 2076 (2013).
- M. Xu, L. Hao, Y. Liu, W. Li, L. Xing, and B. Li, "Experimental and theoretical investigations of dimethylacetamide (DMAc) as electrolyte stabilizing additive for lithium ion batteries." *J. Phys. Chem. C*, 115, 6085 (2011).
- A. Xiao, W. Li, and B. L. Lucht, "Thermal reactions of mesocarbon microbead (MCMB) particles in LiPF₆-based electrolyte." J. Power Sources, 162, 1282 (2006).
- W. Li, A. Xiao, B. L. Lucht, M. C. Smart, and B. V. Ratnakumar, "Surface analysis
 of electrodes from cells containing electrolytes with stabilizing additives exposed to
 high temperature" *J. Electrochem. Soc.* 155, A648 (2008)
- high temperature." *J. Electrochem. Soc.*, **155**, A648 (2008).

 27. L. You, K. Duan, G. Zhang, W. Song, T. Yang, X. Song, S. Wang, and J. Liu, "N, N-dimethylformamide electrolyte additive via a blocking strategy enables high-

- performance lithium-ion battery under high temperature." J. Phys. Chem. C, 123, 5942 (2019)
- C. Liu, T. Li, H. Zhang, Z. Song, C. Qu, G. Hou, H. Zhang, C. Ni, and X. Li, "DMF stabilized Li₃N slurry for manufacturing self-prelithiatable lithium-ion capacitors." Sci. Bull., 65, 434 (2020).
- N. Togasaki, T. Momma, and T. Osaka, "Enhanced cycling performance of a Li metal anode in a dimethylsulfoxide-based electrolyte using highly concentrated lithium salt for a lithium-oxygen battery." J. Power Sources, 307, 98 (2016)
- S. Liu et al., "Inorganic-rich solid electrolyte interphase for advanced lithium metal batteries in carbonate electrolytes." Angew. Chem. Int. Ed., 60, 3661 (2021).
- F. Jeschull, F. Lindgren, M. J. Lacey, F. Björefors, K. Edström, and D. Brandell, "Influence of inactive electrode components on degradation phenomena in nano-Si electrodes for Li-ion batteries." *J. Power Sources*, 325, 513 (2016).
- K. W. Schroder, A. G. Dylla, S. J. Harris, L. J. Webb, and K. J. Stevenson, "Role of surface oxides in the formation of solid-electrolyte interphases at silicon electrodes for lithium-ion batteries." ACS Appl. Mater. Interfaces, 6, 21510 (2014).
- X. Zhang, R. Kostecki, T. J. Richardson, J. K. Pugh, and P. N. Ross, "Electrochemical and infrared studies of the reduction of organic carbonates." *J. Electrochem. Soc.*, 148, A1341 (2001).
- Z. Chen, J. Liu, and K. Amine, "Lithium difluoro(oxalate)borate as salt for lithiumion batteries." *Electrochem. Solid-State Lett.*, 10, A45 (2007).
- S. S. Zhang, "Role of LiNO₃ in rechargeable lithium/sulfur battery." *Electrochim. Acta*, 70, 344 (2012).
- B. S. Parimalam and B. L. Lucht, "Reduction reactions of electrolyte salts for lithium ion batteries: LiPF₆, LiBF₄, LiDFOB, LiBOB, and LiTFSI." J. Electrochem. Soc., 165, A251 (2018).
- S. Jurng, Z. L. Brown, J. Kim, and B. L. Lucht, "Effect of electrolyte on the nanostructure of the solid electrolyte interphase (SEI) and performance of lithium metal anodes." *Energy Environ. Sci.*, 11, 2600 (2018).
- J. Kim, O. B. Chae, and B. L. Lucht, "Perspective-structure and stability of the solid electrolyte interphase on silicon anodes of lithium-ion batteries." *J. Electrochem. Soc.*, 168, 030521 (2021).
- Q. Dong et al., "Insights into the dual role of lithium Difluoro(oxalate)borate additive in improving the electrochemical performance of NMC811llgraphite cells." ACS Appl. Energy Mater., 3, 695 (2020).